The XMM-Newton Iron Line Profile of NGC 3783

J.N. Reeves[1,2], K. Nandra[3], I.M. George[1,4], K.A. Pounds[5], T.J. Turner[1,4], T. Yaqoob[1,6]

jnr@milkyway.gsfc.nasa.gov

ABSTRACT

We report on observations of the iron K line in the nearby Seyfert 1 galaxy, NGC 3783, obtained in a long, 2 orbit ($\sim$ 240 ks) *XMM-Newton* observation. The line profile obtained exhibits two strong narrow peaks at 6.4 keV and at 7.0 keV, with measured line equivalent widths of 120 and 35 eV respectively. The 6.4 keV emission is the Kα line from near neutral Fe, whilst the 7.0 keV feature probably originates from a blend of the neutral Fe Kβ line and the Hydrogen-like line of Fe at 6.97 keV. The relatively narrow velocity width of the Kα line ($\lesssim$ 5000 km s^{-1}), its lack of response to the continuum emission on short timescales and the detection of a neutral Compton reflection component are all consistent with a distant origin in Compton-thick matter such as the putative molecular torus. A strong absorption line from highly ionized iron (at 6.67 keV) is detected in the time-averaged iron line profile, whilst the depth of the feature appears to vary with time, being strongest when the continuum flux is higher. The iron absorption line probably arises from the highest ionization component of the known warm absorber in NGC 3783, with an ionization of log $\xi \sim 3$ and column density of $N_{\rm H} \sim 5 \times 10^{22}$ cm^{-2} and may originate from within 0.1 pc of the nucleus. A weak red-wing to the iron K line profile is also detected below 6.4 keV. However when the effect of the highly ionized warm absorber on the underlying continuum is taken into account, the requirement for a relativistic iron line component from the inner disk is reduced.

---

[1]Laboratory for High Energy Astrophysics, Code 662, NASA Goddard Space Flight Center, Greenbelt Road, Greenbelt, MD 20771, USA.

[2]Universities Space Research Association

[3]Astrophysics Group, Imperial College, Blackett Laboratory, Prince Consort Road, London SW7 2BW, UK.

[4]Joint Center for Astrophysics, University of Maryland, Baltimore County, 1000 Hilltop Circle, Baltimore, MD 21250, USA.

[5]X-ray and Observational Astronomy Group; University of Leicester; Leicester LE1 7RH; UK.

[6]Department of Physics and Astronomy, Johns Hopkins University, Baltimore, MD 21218, USA.

Subject headings: galaxies: active — Seyferts: individual: NGC 3783 — X-rays: galaxies

1. Introduction

NGC 3783 is a bright (V=13 mag), nearby (z=0.00973), Seyfert 1 galaxy, which was first detected in X-rays in the *Ariel-V* all sky survey (McHardy et al. 1981) and subsequently in the high Galactic latitude survey conducted by HEAO-1 (Piccinotti et al. 1982). Since these early X-ray detections, there have been many observations of NGC 3783 in the X-ray band. A ROSAT observation of NGC 3783 showed evidence for a ionized absorber in the soft X-ray spectrum (Turner et al. 1993), which was confirmed during *ASCA* observations (George, Turner & Netzer 1995; George et al. 1998). Subsequent high resolution grating observations of NGC 3783 with *Chandra* and *XMM-Newton* (Kaspi et al. 2000, 2001, 2002; Blustin et al. 2002; Behar et al. 2003) have revealed the soft X-ray absorber with unprecedented accuracy and resolution. Indeed the recent 900 ks observation obtained with the Chandra High Energy Transmission Grating Spectrometer (HETGS) probably represents the best soft X-ray spectrum (in terms of the combination of spectral resolution and signal to noise) obtained on any AGN to date, with the spectrum showing numerous absorption lines from all of the abundant elements between C and Fe, over a wide range of ionization states (Kaspi et al. 2002; Krongold et al. 2003; Netzer et al. 2003).

Our primary aim in this paper is to study in detail the iron K line profile of NGC 3783. The iron Kα emission line diagnostic in AGN first became important during the *Ginga* era, showing that the 6.4 keV iron Kα emission line and associated Compton reflection hump above 7 keV was common amongst Seyfert galaxies (Pounds et al. 1990; Nandra & Pounds 1994). The higher (CCD) resolution spectra available with the *ASCA* satellite appeared to indicate that the line profiles were broad and asymmetrically skewed (to lower energies), which was interpreted as evidence that the majority of the line emission originated from the inner accretion disk around the massive black hole (Tanaka et al. 1995; Nandra et al. 1997; Reynolds 1997). Indeed observations of NGC 3783 with *ASCA* also appeared to show a broad, relativistic iron line profile (Nandra et al. 1997; George et al. 1998), whilst the presence of the higher energy Compton reflection hump in NGC 3783 has been confirmed in a *BeppoSAX* observation (De Rosa et al. 2002).

The picture now emerging from the study of the iron K line with *XMM-Newton* and *Chandra* appears to be much more complex. The presence of a narrower 6.4 keV iron emission component, from more distant matter (e.g. the outer disk, BLR or the molecular torus) appears to be commonplace in many type I AGN including NGC 3783, e.g. Mrk 205 (Reeves et al. 2001); NGC

5548 (Yaqoob et al. 2001); NGC 5506 (Matt et al. 2001); Mrk 509 (Pounds et al. 2002); NGC 3516 (Turner et al. 2002); NGC 4151 (Schurch et al. 2003) and many other objects. In contrast the broad, relativistic component of the iron line profile appears to be much weaker than anticipated (Pounds & Reeves 2002; Reeves 2003) and in some cases may be absent altogether, e.g. NGC 5548 (Pounds et al. 2003a); NGC 4151 (Schurch et al. 2003). Observations have also revealed that highly ionized emission components (from He or H-like iron) may also be present in some, typically higher luminosity AGN, e.g. PG 1116+215 (Nandra et al. 1996); Mrk 205 (Reeves et al. 2001); NGC 5506 (Matt et al. 2001); Mrk 509 (Pounds et al. 2002); Mrk 766 (Pounds et al. 2003b); NGC 7314 (Yaqoob et al. 2003). The situation seems even further complicated, because of the presence of ionized iron K-shell absorption edges and/or lines in some AGN (Nandra et al. 1999; Chartas et al. 2002; Chartas, Brandt & Gallagher 2003; Pounds et al. 2003c; Reeves et al. 2003), which may be associated with high velocity outflows. Furthermore transient, narrow, redshifted Fe line features have been observed in some AGN, e.g. NGC 3516 (Turner et al. 2002); Mrk 766, (Turner et al. 2003), which may be the emission associated with such outflows.

Here we present a study of the iron K-shell line from a long (240 ks) observation of NGC 3783 conducted by *XMM-Newton* in December 2001. The results from a much shorter (40 ks) earlier observation of NGC 3783 by *XMM-Newton* have been published by Blustin et al. (2002), who highlight the complexity of the iron line profile in this object, whilst an analysis of the RGS spectrum from this observation have recently been presented by Behar et al. (2003). Together with the long 300 ks *XMM-Newton* exposure of the Seyfert 1 MCG -6-30-15 (Fabian et al. 2002), the current observation represents the best available dataset with which to study the iron K line profile in AGN, as the long *XMM-Newton* observations offer very high signal to noise up to 12 keV. This allows us to study the various components, such as the narrow and broad lines, the reflection hump above 7 keV and any absorption lines or edges present in the iron K-shell band. The long *XMM-Newton* observation also makes it feasible to probe any changes in the iron K profile and the continuum on relatively short timescales. The higher resolution, but lower signal to noise 900 ks Chandra-HETGS spectrum complements this *XMM-Newton* observation by allowing the study of the narrow emission/absorption lines at higher spectral resolution; detailed modeling of the iron K band in this non-simultaneous dataset will be presented in another paper (Yaqoob et al. 2003, in preparation).

In Section 2, the *XMM-Newton* observations of NGC 3783 are outlined, whilst in Section 3 the detailed modeling of the time-averaged iron K line profile is performed. In Section 4 the effect of the warm absorber on the iron line profile is investigated, whilst in Section 5 we discuss the variability of the iron K-shell band and continuum over the observation.

2. The XMM-Newton Observations

NGC 3783 was observed by *XMM-Newton* between 17-21 December 2001 over 2 complete satellite orbits, with a total good exposure of just over 240 ks with the EPIC (European Photon Imaging Camera) detectors. Data was taken with the EPIC-pn detector (Struder et al. 2001) in Small Window Mode and with the EPIC-MOS detectors (Turner et al. 2001) in Full Window mode and timing mode. The data was reduced using version 5.4 of the XMM-SAS software using the standard processing scripts (EMCHAIN and EPCHAIN). Only short time intervals were excluded during the end of each satellite orbit, due to high count rate background flares, the background rates were nominal for the remainder of the observation. Data were selected using event patterns 0-12 (for the MOS) and pattern 0-4 (for the pn) and only good X-ray events (using the selection expression 'FLAG=0' in EVSELECT) were included. The spectra were extracted from circular source regions of 40″ radius, whilst background spectra were extracted from an offset circle of identical size, close to NGC 3783, but free of any background sources. Response matrices and ancillary response files were generated using the SAS tasks RMFGEN and ARFGEN respectively. The time-averaged, 0.2-12 keV flux of NGC 3783 during the observation was 6.8×10^{-11} ergs cm^{-2} s^{-1}. The EPIC-pn lightcurve extracted over the full 0.2-12.0 keV band for both orbits is shown in Figure 1.

Unfortunately none of the MOS data taken during the observation are suitable for detailed spectral analysis, as the full window observations are heavily piled up at the flux level of the source, whilst the MOS timing modes are not presently calibrated to sufficient accuracy. Conversely the EPIC-pn exposures taken in Small Window mode do not suffer from significant pile-up, at the level of $< 2\%$ of events. Thus the spectral analysis was restricted to the EPIC-pn detector, which provides the highest signal to noise ratio in the iron K-shell band up to 12 keV. Background subtracted spectra were fitted using XSPEC v11.2, including data over the energy ranges 0.3 to 12 keV. A Galactic absorption column of $N_H = 8.5 \times 10^{20}$ cm^{-2} (Dickey & Lockman 1990) was included in all the fits and fit parameters are quoted in the rest-frame of NGC 3783 at z=0.00973. Given the large number of counts available in the observation, the source spectra were binned to a minimum of 50 counts per bin to enable the use of the χ^2 minimization process when performing X-ray spectral fits. All errors are quoted at 90% confidence for one interesting parameter (corresponding to $\Delta\chi^2 = 2.7$).

2.1. Initial Spectral Fits

Initially we concentrate our analysis on the time-averaged NGC 3783 spectrum, from the whole 240 ks observation, which provides us with the highest signal to noise, especially important for studying the iron K-shell band in the greatest detail. A time dependent analysis is described

in Section 5, which shows that any temporal spectral changes are subtle, and do not effect our conclusions about the mean iron line profile. Initially a single power-law was fitted over a relatively clean part of the EPIC-pn spectrum between 3.5-5 keV, i.e. avoiding the iron line above 5 keV and the strong warm absorber in the soft X-ray part of the spectrum. The best-fit photon index was $\Gamma = 1.6$, whilst the spectrum and data/model residuals (Figure 2) show a clear deficit of counts between 0.7 and 3 keV, due to the known soft X-ray warm absorber in NGC 3783, whilst strong residuals are also present above 6 keV in the iron K-shell emission/absorption band. A weak soft X-ray excess is also present at the lowest energies below 0.7 keV, which has also been detected in an earlier *BeppoSAX* observation (De Rosa et al. 2002).

In order to model the iron K shell band we concentrate our analysis on the higher energy portion of the spectrum. The exact value of the low energy cut-off used is important, as the aim is to analyze part of the spectrum which is largely unaffected by the strong soft X-ray warm absorber, which can have a considerable effect in the determination of the underlying continuum. Inspection of Figure 2 shows that the absorber starts to have a significant effect below 3 keV in the EPIC-pn data. We have also studied the (non-simultaneous) 900 ks Chandra-HETGS observation presented by Kaspi et al. (2002). All the strong absorption features in this spectrum are present below 4.5 Angstrom (2.8 keV) mainly due to K-shell absorption lines from elements between C and S, as well as L-shell absorption from iron. The last abundant element that may contribute discrete spectral features in the soft X-ray absorber is Ar, the HETGS spectrum shows that there are weak absorption lines due to He and H-like Ar at 3.1 and 3.3 keV respectively.

In order to minimize the effect of the warm absorber when analyzing the iron K line profile, we adopt a conservative approach, and restrict our spectral analysis to the energy range from 3.5 to 12 keV. Over this band the only discrete absorption features (other than from iron) are due to Ca XIX and Ca XX, which are extremely weak even in the 900 ks HETGS observation and are not a significant source of opacity in the EPIC-pn spectrum. In a later section of this paper (Section 4) we also discuss the effect the warm absorber may have on the continuum (through bound-free absorption) and above the neutral iron K-shell edge, by comparing our fits with models generated with the photo-ionization code XSTAR (Kallman et al. 1996).

3. The Time-Averaged Iron line Profile of NGC 3783

Initially we fitted the hard band (3.5-12 keV) EPIC-pn spectrum with a simple power-law together with neutral absorption from our own Galaxy. The fit was very poor ($\chi^2/dof = 3719/1292$), with a best-fit photon index of $\Gamma = 1.58 \pm 0.01$. All the fit parameters are listed in Table 1. The data/model residuals are plotted in Figure 3 (panel a), two strong emission lines are apparent close to 6.4 keV and 7.0 keV, as well as a deficit of counts both near 6.6-6.7 keV and above the neutral

iron K edge at 7 keV, whilst a small excess of counts is observed red-wards of the 6.4 keV line.

As a first step, we model the two strong emission lines with simple Gaussian profiles (Table 1, fit 1), with the energy, width and line flux free parameters (in addition to the continuum photon index and normalization). The line centroids are at 6.39 ± 0.01 keV and 7.00 ± 0.02 keV, with equivalent widths of 123 ± 6 eV and 34 ± 5 eV and fluxes of $(5.9 \pm 0.3) \times 10^{-5}$ erg cm^{-2} s^{-1} and $(1.4 \pm 0.3) \times 10^{-5}$ erg cm^{-2} s^{-1} respectively. The 1σ widths of the 6.4 and 7.0 keV lines are 57 ± 8 eV and 53 ± 23 eV respectively, which correspond to FWHM velocity widths of ~ 6100 km s^{-1} and ~ 5200 km s^{-1} respectively. Note that the non-zero widths of the lines are *required* by the data, for the $K\alpha$ line the improvement in fit statistic is $\Delta\chi^2 = 81$ for allowing the width to be non-zero (corresponding to an F-test null hypothesis probability of 1.3×10^{-15}). We comment on possible origins of the width of the 6.4 keV line later.

The observed ratio of the line fluxes are approximately 4:1, whereas one would expect a ratio of 150:17 between the $K\alpha$ and $K\beta$ transitions from neutral iron. Thus there is likely to be an extra component contributing towards the emission line at 7.0 keV. Indeed the line energy of the 7.0 keV line is in between the lab frame energies for Fe XXVI Lyα and Fe I Kβ, which indicates that this line is a blend of these two emission lines (and which may in part account for the velocity width of this line component). In order to determine the strength of the putative H-like iron line, we fixed the ratio of the intensity of the $K\beta$ line at 7.06 keV to 17/150 of that of the Fe Kα line at 6.4 keV. We also tied the velocity widths of the all 3 emission lines to that of the 6.4 keV line (Table 1, fit 2). Indeed a H-like Fe line component is required in the fits ($\Delta\chi^2 = 52$ for 2 extra degrees of freedom), the measured energy of 6.96 ± 0.02 keV is very close to the known rest-frame energy for Fe XXVI at 6.966 keV (Pike et al. 1996), whilst the equivalent width of the line is 20 ± 5 eV.

Overall the fit statistic for this three component emission line fit (with $\chi^2/dof = 1591/1287$) is not formally acceptable, corresponding to a null hypothesis probability of 1.15×10^{-8}. The data/model residuals to this fit are shown in Figure 3b, clearly there is a broad excess (red-wing) below 6.4 keV, whilst there appears to be an absorption line in the data near 6.6-6.7 keV. A strong Compton reflection component may also be present, as indicated in the spectrum by an edge above 7 keV and spectral hardening up to 12 keV. Indeed one would expect a Compton hump to accompany the 6.4 keV iron K emission line, if the line results from reprocessing in Compton-thick matter. Thus a neutral Compton reflection component, the PEXRAV model in XSPEC (Magdziarz & Zdziarski 1995), was added to the model. The strength of the reflection component (measured by the parameter $R = \Omega/2\pi$, where Ω is the solid angle in steradian covered by the reflecting material) was initially fixed at $R = 1$, with an inclination of 30°and a cut-off energy of ~ 250 keV using solar abundances. Note these parameters are consistent with the measurement of a Compton hump in an earlier *BeppoSAX* observation (De Rosa et al. 2002), where the strength of the reflection component was measured to be $R \sim 0.8$ with a cut-off energy of about 300 keV. After adding the Compton

reflection component, the fit statistic improves considerably ($\chi^2/dof = 1492/1287$), whilst all 3 emission lines are still required in the dataset (Table 1, fit 3). The underlying power-law slope is now steeper ($\Gamma = 1.73 \pm 0.01$), accounting for the soft excess observed in the broad-band EPIC-pn spectrum. After allowing the strength of the reflection component to vary, we obtain $R = 1.6 \pm 0.3$, with a steeper photon index ($\Gamma = 1.78 \pm 0.01$). However as the exact value of R is very dependent on the high energy calibration of the EPIC-pn above 8 keV, we proceed by fixing R to 1, which is consistent with the strength of the Fe Kα line measured in the spectrum (George & Fabian 1991) and the measurement of the reflection hump by *BeppoSAX* (De Rosa et al. 2002).

After adding the reflection component to the spectral fit the excess of counts below 6.4 keV and the absorption line near 6.7 keV are still apparent in the residuals (Figure 3c). To model the apparent red-wing to the Fe Kα line we added a 'Diskline' component (Fabian et al. 1989), to represent the emission from the inner accretion disk around a Schwarzschild black hole, taking the inner and outer radii of the disk as $6R_S$ and $100R_S$ respectively (where $R_S = 2GM/c^2$) and fixing the rest-energy of the diskline emission at 6.4 keV. The improvement in fit statistic upon adding the diskline component is substantial ($\Delta\chi^2 = 112$ for 3 additional parameters). The emissivity (β) of the diskline (where the disk emission varies with radius as $R^{-\beta}$) was $\beta = 3.3 \pm 0.5$, the inclination angle derived was $19 \pm 9°$ whilst the strength of the line is relatively weak (the equivalent width is 58 ± 12 eV).

The spectral fit was improved further by the addition of a narrow (unresolved by EPIC-pn) absorption line at 6.67 ± 0.04 keV, with an equivalent width of 17 ± 5 eV. Note the other iron emission line components are required as in the previous fits (Table 1, fit 4). The absorption line component is unambiguously required in the model fit with a high degree of statistical significance ($\Delta\chi^2 = 56$ for 2 additional degrees of freedom), equivalent to an F-test null hypothesis probability of 2.9×10^{-12}. The absorption line cannot be modeled with another emission component, such as the blue-wing of the disk emission line for instance, as the line is observed below the level of the power-law continuum (e.g. see Figure 3, panel c and d). The energy of this absorption line component probably corresponds to a blend of several lines of highly ionized iron, e.g. Fe XXIII at 6.62 keV, Fe XXIV at 6.66 keV and Fe XXV at 6.70 keV. Overall the fit statistic ($\chi^2/dof = 1324/1282$) is now formally acceptable, no other spectral components are required.

3.1. The Width of the 6.4 keV Fe line

After modeling all the emission and absorption line components, and taking into account the resolution of the EPIC-pn detector (through the pn re-distribution matrix), the best fit 1σ width of the 6.4 keV Kα line is $\sigma = 52 \pm 10$ eV. In terms of the FWHM width, this corresponds to 120 ± 23 eV or 5600 ± 1100 km s^{-1} and appears to be just resolved by the EPIC-pn detector (see

Figure 4). Note that the neutral Fe Kα line is actually a blend of two lines, at 6.391 keV and 6.404 keV, with a branching ratio of 2:1. However taking this into account in the spectral fits has a negligible effect on the velocity width of the line.

We note that this velocity width is broader than that reported by Kaspi et al. (2002) from the 900 ks Chandra HETGS observation. However some caution should be exercised when interpreting the velocity width obtained from the lower resolution EPIC-pn spectrum (FWHM resolution $\Delta E \sim$ 120 eV at 6 keV) compared to the higher resolution HETGS spectrum ($\Delta E \sim 35$ eV at 6 keV). For instance the 6.4 keV line may appear to be slightly broader, as the EPIC-pn is largely unable to resolve the first Compton scattering shoulder of this line (at 6.29 keV), which is apparent in the HETGS data (Yaqoob et al. 2003, in preparation). In addition, some contribution from a weak outer disk emission line component may also contribute towards the width of the EPIC-pn line. Thus the quoted velocity width of ~ 5600 km s^{-1} should be regarded as an upper limit. Nonetheless the width of the line is consistent with the bulk of the line flux originating from the broad line region (BLR); in NGC 3783 the typical FWHM velocity dispersion in the BLR is ~ 4000 km s^{-1} (Riechert et al. 1994; Wandel, Peterson & Malkan 1999). However some contribution from further out, such as the the outer BLR or molecular torus, cannot be discounted.

4. The Effect of the Warm Absorber

Whilst measuring the iron K line profile is our primary aim in this paper, it is important to verify whether the deep soft X-ray warm absorber in NGC 3783 absorber has any effect on the high energy spectrum and the iron line profile. The warm absorber could introduce subtle spectral curvature below 6.4 keV, and there may be some additional opacity above the neutral iron K-shell edge at 7.1 keV. Whilst this will have little effect on modeling the narrow Fe emission line components, the effect on the weak, broad red-wing (which constitutes only 5% of the continuum at 6 keV) may be crucial. Furthermore there is direct evidence for a high ionization component of the warm absorber in the iron K-shell band, through the detection of a strong 6.7 keV absorption line.

As a starting point, we base our initial models on those of Blustin et al. (2002), who fit the RGS spectra from an earlier, short (40 ks) *XMM-Newton* observation of NGC 3783. Conveniently, these authors parameterized their model in terms of a two zone warm absorber; a high ionization component responsible for the He and H-like K-shell absorption lines from the abundant soft X-ray elements (e.g. C, N, O, Ne, Mg) as well as L-shell absorption from highly ionized iron (Fe XVII-XXIV), with a low ionization component responsible for the unresolved transition array (UTA) resulting from a blend of inner-shell $2p \rightarrow 3d$ absorption lines from Fe M-shell ions. Although this model parameterizes an earlier observation, it is thought that the warm absorber in NGC 3783

is relatively stable over time, as shown recently by Behar et al. (2003), who argue that the most recent RGS spectra from the long *XMM-Newton* look agree well with this earlier Blustin et al. (2002) model. A similar conclusion has been reached by Netzer et al. (2003) from a detailed analysis of all the Chandra observations over time of this source.

In order to duplicate this soft X-ray absorption as closely as possible, we generated two grids of XSTAR photoionization models with similar parameters to those used in the Blustin et al. (2002) model. The relative elemental abundances of C through to Fe quoted in Blustin et al. (2002) were used, together with an outflow velocity of 800 km s^{-1} and a (1σ) turbulence velocity of 500 km s^{-1}. As per Blustin et al. (2002), for the low ionization component we use an iron over-abundance of 10 times solar, and then fix the column density and ionization parameter at $N_{\rm H} = 6 \times 10^{20}$ cm^{-2} and $\log \xi = 0.3$ erg cm s^{-1} respectively. Note however that this low ionization component is only added for completeness, it has relatively little effect on the high energy spectrum above 3.5 keV, only adding a small amount of opacity near the neutral iron K edge at 7.1 keV. For the higher ionization component, we initially fix the column density at $N_{\rm H} = 3 \times 10^{22}$ cm^{-2} with an ionization parameter of $\log \xi = 2.4$, using solar abundances of iron.

This model was then applied to the EPIC-pn spectrum over the 3.5-12 keV bandpass. Two narrow emission line components (one representing Fe Kα, the 2nd representing the blend of Fe Kβ and Fe XXVI) were included in the fit, as well as the reflection component (with R fixed at 1) and the power-law continuum. Neither the diskline component nor the absorption line at 6.7 keV were included in the model. Initially the fit is poor ($\chi^2/dof = 1528/1287$), the model does not reproduce the energy and depth of the strong 6.7 keV absorption line present in the data, as the ionization state of even the higher ionization absorber is not sufficient to produce the required column of highly ionized iron (e.g. Fe XXIII–XXV).

Thus, to fit the Fe K-shell absorption line present in the *XMM-Newton* EPIC data, we allowed the ionization parameter and column density of the highest ionization absorption component to vary. A higher ionization parameter of $\log \xi = 2.9 \pm 0.3$ erg cm s^{-1} is required, whilst the column density is now $N_{\rm H} = (4.6 \pm 0.8) \times 10^{22}$ cm^{-2} and the underlying continuum slope is $\Gamma = 1.69 \pm 0.01$. The fit to the spectrum has significantly improved ($\chi^2/dof = 1332/1284$), reproducing the depth of the 6.7 keV absorption line well (see Figure 5), as the ionization state of the absorber is now high enough for Fe XXIII–XXV to be the dominant ions present.

Therefore this high ionization absorber, which is responsible for the resonant iron absorption line, probably represents the highest ionization component of the known warm absorber in NGC 3783, in addition to the lower ionization components responsible for the soft X-ray absorber, as measured by Blustin et al. (2002) and Kaspi et al. (2002) in the *XMM-Newton* RGS and *Chandra* HETGS spectra respectively. Note that extrapolating this best fitting high ionization model to lower energies (0.3 keV), but also including the lower ionization (with $\log \xi \sim 2.4$ and $\log \xi \sim 0.3$)

warm absorber components modeled by (Blustin et al. 2002), gave a reasonable fit to the broad-band (0.3-12 keV) EPIC-pn spectrum. The overall fit statistic was $\chi^2/dof = 2641/1894$, whilst the broad-band spectrum, and data/model residuals to the warm absorber model, are plotted in Figure 6. The remaining residuals present in the spectrum are small, at the 5% level, similar to the residual calibration uncertainties in the EPIC-pn responses. The continuum photon index returned was $\Gamma = 1.67 \pm 0.01$, whilst a weak soft excess modeled by a black-body with a temperature of $kT = 97 \pm 4$ eV was required to fit the very softest part of the spectrum.

Interestingly, with the addition of the warm absorber, there is now no longer any requirement for the broad, relativistic disk emission component, the fit statistic is not significantly improved upon the addition of a diskline component, as the residuals to the warm absorber fit are small. (Note that the existence of the narrow Fe emission components are not affected). Formally the 90% upper-limit on a disk emission line component is < 35 eV, assuming a disk emissivity of $\beta = 3$ and an inclination angle of 30°.

In order to assess directly the effect of the warm absorber on the high energy spectrum, we removed the warm absorber components from the model. The result is shown in Figure 7, clearly one can see the contribution that the high ionization absorber makes towards the 6.7 keV absorption line. However the absorber also introduces some continuum curvature below the iron K line (which effects the fits to the broad line component), whilst there is also some opacity from 7-9 keV due to iron K-shell bound-free absorption, with an optical depth $\tau \lesssim 0.1$. This is also illustrated in Figure 8, which plots the highest ionization component of the warm absorber model, normalized to a $\Gamma = 2$ power-law continuum. One can clearly see the continuum curvature between 3-6 keV, due to recovery from highly ionized K-shell edges from Mg, Si and S as well as from the L-shell edges of Fe below 3 keV. Additional opacity is also present above 8 keV, due to a blend of iron K-shell edges, as well the Kβ (and higher series) absorption lines of highly ionized iron.

5. Variability of the Fe line and hard X-ray continuum

Initially we split the observation according to the two separate *XMM-Newton* orbits (e.g. Figure 1). The time-averaged flux state was relatively low during the first orbit (3.5-10 keV band flux of 2.77×10^{-11} erg cm^{-2} s^{-1}) and higher during the 2nd orbit (3.5-10 keV band flux of 3.69×10^{-11} erg cm^{-2} s^{-1}). As in the earlier fits, the iron K-shell spectral features were parameterized by multiple Gaussian emission/absorption line components and a neutral reflector (with $R = 1$). A slight steepening with flux of the hard power-law index was observed, from $\Gamma = 1.62 \pm 0.01$ in the first orbit to $\Gamma = 1.68 \pm 0.01$ during the 2nd orbit. However there was no change in the 6.4 keV Fe Kα line parameters, the Fe line flux being consistent with a constant value ($5.7 \pm 0.4 \times 10^{-5}$ photons cm^{-2} s^{-1} during the first orbit and $5.4 \pm 0.5 \times 10^{-5}$ photons cm^{-2} s^{-1} during the 2nd orbit).

These values are also consistent with the Fe Kα flux measured in the long Chandra HETGS observation, of $5.3 \pm 0.6 \times 10^{-5}$ photons cm^{-2} s^{-1} (Kaspi et al. 2002). Note, given the much poorer statistics on the 7.0 keV line, it is not possible to determine whether or not this line component varied.

However, a significant change in the 6.7 keV absorption line was observed from one orbit to the next, indicating that the highly ionized absorber is variable on timescales of $\sim 10^5$ s. This is illustrated in Figure 9, which shows the ratio to the best fit model to the data (but not including the absorption component) for the two orbits. Thus the absorption line appears to be strongest during the second, higher flux orbit (with an equivalent width of 18 ± 4 eV), whilst it was barely detected during the first orbit (equivalent width of 7 ± 4 eV).

The observations were also split into shorter time segments, of 8×30 ks duration (i.e. 4 segments per orbit). However the more limited photon statistics do not enable us to determine whether the 6.7 keV absorption line is variable over this shorter timescale. However a similar pattern was seen with regards to variability of the Fe Kα line and the continuum. Whilst the 3.5-10 keV continuum flux varied by as much as 50% during the observation, there was no change in the iron Kα line flux (to within 10% of the mean value). Similarily, a change in continuum photon index was observed, steepening from $\Gamma = 1.57 \pm 0.02$ at the lowest flux level to $\Gamma = 1.71 \pm 0.02$ at the highest flux level. This is consistent with the well known positive Flux-Gamma correlation found in many active galaxies. An alternative interpretation is that the primary power-law index may infact be the same for the different flux states. However if the Compton reflector originates from distant matter and does not respond to the continuum (which appears consistent with the constant-flux Kα emission line), then this component will appear stronger relative to the weaker power-law in the low flux spectra, resulting in a harder spectrum overall.

6. Discussion and Conclusions

The long *XMM-Newton* observation of the bright, Seyfert 1 galaxy NGC 3783 has revealed a complex iron K line profile above 3.5 keV. Two strong, but relatively narrow emission lines are apparent at 6.4 and 7.0 keV, the former from the (near) neutral Fe Kα fluorescence line, whilst the latter is likely to be a blend of the neutral Fe Kβ line as well as a component from hydrogenic iron (i.e. Fe XXVI Ly-α). The observations also revealed a weak red-wing to the iron Kα line profile below 6.4 keV, as well as an unambiguous detection of a high ionization iron absorption line at 6.7 keV.

6.1. The Nature of the Iron K Line Emission in NGC 3783

The 6.4 keV Fe Kα line appears to be resolved in the EPIC-pn spectrum, with a typical (FWHM) velocity width of $\sim$ 5000 km s^{-1}. At first glance this velocity is consistent with the FWHM dispersion in the BLR of NGC 3783 (Riechert et al. 1994; Wandel, Peterson & Malkan 1999). However we note that the velocity width determined by the higher spectral resolution Chandra HETGS observation is much lower, the core of the 6.4 keV line having a FWHM width of $\sim$ 1800 km s^{-1} (Kaspi et al. 2002). One possible explanation for this apparent discrepancy is the lower spectral resolution of the EPIC-pn detector compared to the HETG. For instance at the EPIC-pn resolution ($\Delta E \sim 120$ eV at 6 keV), it is difficult to resolve the narrow core of the line from a broader component, such as the Compton scattering shoulder of the line, which is apparent in the Chandra line profile (Yaqoob et al. 2003, in preparation).

Indeed the detection of the Compton scattering shoulder in the Chandra line profile, as well as the narrow width of the line core is indicative of scattering in distant Compton thick matter. Additionally both the *XMM-Newton* and the earlier *BeppoSAX* (De Rosa et al. 2002) observations also require a strong ($R \sim 1$) Compton reflection component above 7 keV. However the line is unlikely to originate from the disk unless the typical radius is $> 1000R_s$. Furthermore line does not respond to the continuum within the timescale (days) of the *XMM-Newton* observation in December 2001, whilst the line flux also does not appear to vary within the 18 month timescale of the Chandra observations between 21 January 2000 and 26 June 2001 (Yaqoob et al. 2003, in preparation), or indeed between the Chandra observations and the December 2001 *XMM-Newton* observation (the mean line flux from Chandra, of $5.3 \pm 0.6 \times 10^{-5}$ photons cm^{-2} s^{-1}, Kaspi et al. 2002, is consistent with the *XMM-Newton* value). Given the lack of variation on these timescales, the bulk of the 6.4 keV line would appear to originate from distant matter. In the context of AGN unification schemes (Antonucci 1993), one possible source for this distant, Compton-thick reprocessor is the putative molecular torus. Indeed predictions show that the putative torus may be a major contributer towards both the 6.4 keV line commonly seen in the Seyfert 1 spectra from both *XMM-Newton* and *Chandra* observations, as well as the strong iron lines observed in Seyfert 2s (Ghisellini, Haardt & Matt 1994). Other geometries are also possible such as scattering off the Compton thick component of any quasar outflow (Elvis 2000).

Whilst the detection of a narrow and distant 6.4 keV iron line now appears robust in this and many of the Seyfert 1s, generally the presence of the broad iron K line from the inner accretion disk (Tanaka et al. 1995; Nandra et al. 1997) is subject to considerable debate, the broad red-wing being much weaker than anticipated in the new *Chandra* and *XMM-Newton* datasets, for instance in NGC 5548 (Pounds et al. 2003a) or NGC 4151 (Schurch et al. 2003). If a disk-line component is present in NGC 3783 it is very weak, with an equivalent width of only 60 eV even before the warm absorber was modeled.

However, once the high ionization absorber responsible for the Fe K-shell absorption is accounted for in NGC 3783, then the requirement for a broad line is further reduced, with a formal upper-limit of < 35 eV on the equivalent width of such a component. The reduction in strength of the broad line is mainly due to the fact that the absorber can introduce subtle continuum curvature in the X-ray spectrum, even in the iron K-shell band (e.g. see Figures 7 and 8). Indeed this current study may have implications for the detection of the broad iron Kα line in other AGN, which also have a strong ionized absorbers (for instance in NGC 4151 or MCG -6-30-15). In the case of MCG -6-30-15, the broad line component is much stronger (Tanaka et al. 1995; Wilms et al. 2001; Fabian et al. 2002) and its detection appears to be more robust to the spectral model and underlying continuum slope that is assumed (Reynolds et al. 2003; Vaughan, Fabian & Iwasawa 2003). However, the wealth of data now available through the *XMM-Newton* and *Chandra* archives clearly call for a more thorough, systematic analysis of the iron line profile in many AGN.

Indeed an important question is why the broad line is not required in many of the *XMM-Newton* Seyfert 1 spectra, and particularly in NGC 3783, which represents one of the highest quality iron line profiles obtained on any AGN to date? One possibility is that the inner disk is truncated, however given the observed width of the 6.4 keV line (~ 5000 km s^{-1}), this requires that the bulk of the line emission occurs out at radii $> 1000R_s$. However, at such a distance from the black hole, there is unlikely to be substantial hard X-ray emission. Another scenario which is perhaps more realistic is that the inner disk is strongly photoionized, so that most of the iron at the disk surface is fully ionized, and the subsequently the line is too weak to be detected. The magnetic flare model proposed by Nayakshin & Kallman (2001), where the X-ray flux is concentrated in small, intense regions above the disk, can produce a very highly ionized skin at the local disk surface (with a high Compton temperature). The signature of this is a very weak iron line and reflection component, particularly when the underlying photon index is hard ($\Gamma < 2$). One possibility is that the weak emission from Fe XXVI observed in this spectrum is the signature of this highly ionized disk reprocessor. Note that an emission component from Fe XXVI has already been observed in the Chandra HETGS spectrum of the Seyfert 1 NGC 7314 (Yaqoob et al. 2003), which is variable on short timescales, indicating emission from close to the central engine. Furthermore weak, He-like iron lines have also been detected in a some higher luminosity AGN, e.g. PG 1116+215, Nandra et al. (1996); Mrk 205, Reeves et al. (2001); Mrk 509, Pounds et al. (2002). Thus it seems plausible that the inner disk reprocessor in many AGN may be highly ionized, to the extent that in some cases the lines are undetectable.

6.2. The Origin of the Variable, Highly Ionized Iron Absorber

Perhaps the most intriguing finding from this observation is the discovery of a variable absorption line component from highly ionized iron. The observed energy of the line (6.67 ± 0.04 keV) is consistent with the $1s \rightarrow 2p$ transitions of Fe XXIII (6.630 keV), Fe XXIV (6.659 keV) and Fe XXV (6.702 keV) at the systemic velocity of NGC 3783. These transitions all have similar oscillator strengths ($f_{osc} \simeq 0.6$–0.7), hence the observed feature could be a blend of these ions. This absorber may represent the highest ionization phase of the gas that is responsible for the soft X-ray absorber in NGC 3783.

However, recent studies indicate that the lower ionization absorption components in NGC 3783 (Behar et al. 2003; Netzer et al. 2003) responsible for the soft X-ray absorber, do not vary, implying that this absorbing matter is located at large, parsec scale distances. The detection of rapid variability in the iron absorber within the *XMM-Newton* observation does not appear consistent with this; it is possible that the high ionization absorber is a physically separate component, located closer to the nucleus. In order to provide a zeroth order estimate for the location of the high ionization absorber, we calculated the *maximum* possible distance to the iron absorber, on the condition that $\Delta R/R < 1$, i.e. its thickness (ΔR) cannot exceed its distance (R) from the nucleus. Combining the equations $N_{\rm H} = n\Delta R$ and $\xi = L/nR^2$ yields $R < L/N_{\rm H}\xi$. Now as $L = 10^{43}$ erg s^{-1}, $N_{\rm H} = 5 \times 10^{22}$ cm^{-2} and $\xi = 10^3$ erg cm s^{-1}, then the maximum distance of the absorber is 2×10^{17} cm, or < 0.1 pc from the nucleus.

The *XMM-Newton* observations show that the Fe absorption line is variable on timescales of $t_{\rm var} \lesssim 10^5$ s. One possibility is that the variation in depth of the absorber between the two orbits may arise through changes in the ionization state of iron due to an increase in the illuminating flux. In the optically-thin limit, Fe XXIII–XXV are the dominant ions over a wide range of ξ ($400 \lesssim \xi \lesssim 1600$ erg cm s^{-1}). However the lack of significant absorption observed from the $1s \rightarrow 2p$ transition of Fe XXVI (6.966 keV) implies an ionization parameter may be towards the lower end of this range. For instance, if $\xi \sim 6 \times 10^2$ erg cm s^{-1}, then the relative ionization fractions (f_{ion}) will be 0.06, 0.40, 0.31 and 0.14 for Fe XXVI, Fe XXV, Fe XXIV, and Fe XXIII respectively (and $f_{ion} << 0.05$ for the less-ionized species). With such an ionization structure, a reasonable fit to the absorption feature detected in the 2nd-orbit is obtained (see Figure 10, panel a) for a total column density of Fe $N_{\rm Fe} \simeq 3 \times 10^{17}$ cm^{-2} (corresponding to $N_{\rm H} \sim 10^{22}$ cm^{-2} for an Fe abundance $A_{\rm Fe} = 2.7 \times 10^{-5}$, Wilms, Allen & McCray (2000)), assuming ionization equilibrium has been reached.

Now let us consider the 1st-orbit, when the observed intensity of the source was a factor ~ 1.3 lower. In the simplest case, when the absorbing gas is far from the nucleus and sees the same continuum as ourselves, then the ratio of the illuminating flux (and hence ξ) between the 2nd- and 1st-orbits is also 1.3. However such a situation is rejected by the data: Fe XXV, Fe XXIV, and Fe XXIII ions would still be the dominant Fe ions (with $f_{ion} = 0.22$, 0.28 and 0.22, respectively)

resulting in a predicted absorption blend stronger than observed. However the observed hard X-ray continuum is likely to be a composite of the variable *primary* continuum from the central engine and a constant *reflected* continuum from distant matter. This reflection component is observed in the high energy *XMM-Newton* spectrum, through the detection of a strong narrow Kα line and a Compton hump above 7 keV; hence the flux change in the primary continuum emission may be higher, by as much as a factor of two. Indeed a satisfactory model (Figure 10, panel b) can be obtained if we decrease the ionization state further in the first orbit by reducing ionization parameter to $\xi \sim 3 \times 10^2$ erg cm s^{-1}, i.e. by a factor 2 compared to that during the 2nd-orbit. Under these circumstances Fe XXIII and Fe XXII are the dominant ions (with $\lesssim 20\%$ of the Fe in the form of Fe XXIV and above see Figure 10, panel c). Due to the lower oscillator strengths of Fe XXII and below, a weaker line is predicted which is in agreement with the data.

The above example calculations assume ionization equilibrium. One can then consider the circumstances under which this might be true. Specifically, one can calculate the ionization timescale (t_{ion}) required so that sufficient ionizing photons arrive and are absorbed by the gas such as to raise the ionization structure of the gas by the required amount. The column density of a given Fe ion is simply $N_{ion} = f_{ion} N_{\rm Fe}$ and for the underlying continuum appropriate for NGC 3783, 90% of the ionizing photons will be absorbed within a band of width $\Delta E \simeq 0.8 E_{\rm th}$, where $E_{\rm th}$ is the threshold energy. For Fe XXIV, the relavent threshold energy will be at 2.05 keV, i.e corresponding to the L-shell edge energy of Fe XXIV. If the number of photons emitted by the source at $E_{\rm th}$ is $N_i(E_{\rm th})$, and the distance to the absorber is R, then the number of photons absorbed (per unit area) by a given ion within the gas in a time $t_{\rm ion}$ is $N_i(E_{\rm th}) \Delta E \; t_{\rm ion} \; (1 - e^{-\tau})/(4\pi R^2)$, where $\tau = \sigma_{\rm th} N_{ion}$ and $\sigma_{\rm th}$ is the cross-section at the threshold energy.

Equating this to N_{ion} then defines t_{ion} for that ion. Requiring $t_{ion} \leq t_{\rm var}$ then leads to an upper limit on R such that the ionization state of the absorber is able to react to variations in illumination within $t_{\rm var}$. For the ions of interest noted above (i.e. Fe XXI–XXIV), and assuming a distance of 42 Mpc towards NGC 3783, then the ionization equilibrium can be achieved in the 10^5 s timescale between the 1st- and 2nd-orbits if $R \lesssim 0.02$ pc. This is significantly smaller than the parsec-scale distances derived for the soft X-ray absorber (Behar et al. 2003; Netzer et al. 2003), but is consistent with the $\Delta R/R$ estimate above.

Another possibility is that this absorber is similar to the extreme, high velocity ($v \sim 0.1c$) iron absorbers recently observed in some AGN by *XMM-Newton* and *Chandra*, e.g. APM 08279+5255 (Chartas et al. 2002); PG 1211+143 (Pounds et al. 2003c); PG 1115+080 (Chartas, Brandt & Gallagher 2003); PDS 456 (Reeves et al. 2003). These outflows may arise from the innermost part of a disk driven wind (Proga, Stone & Kallman 2000; King & Pounds 2003). In this case the variation seen in the Fe absorber may be due to the passage of ionized matter across the central X-ray source. For a given size of the X-ray emitting region in NGC 3783 one can estimate the distance

of the transient absorbing material passing in front of the central engine, assuming that this occurs on the timescale of the variation seen in the iron absorption line, i.e. $\sim 10^5$ s. In NGC 3783 the estimated black hole mass, obtained through BLR reverberation mapping, is $\sim 10^7$ $M_\odot$ (Onken & Peterson 2002), thus a typical size for the X-ray emitting region is $\sim 20GM/c^2 = 3 \times 10^{13}$cm. Thus the velocity of the absorbing matter passing in front of the source in 10^5 s is $v \sim 3000$ km s^{-1} (or $0.01c$). If one equates this velocity to the escape velocity of the matter at a given radius R from the black hole, then the distance of the absorber is $R \sim 10^{16}$ cm. From the definition of the ionization parameter, $L_x/\xi = nR^2$, whilst from observation $L_x = 10^{43}$ erg s^{-1} and $\xi = 10^3$ erg cm s^{-1}, hence the density of the absorbing matter is $n \sim 10^8$ cm^{-3}

Note that the physical parameters of the highly ionized iron absorber in NGC 3783 are somewhat less extreme than in some of the more luminous quasars noted above, i.e. the column density is a factor of 10 lower, whilst no large velocity shift in the iron absorption line is observed in NGC 3783. This may indicate we are observing the outflow at a greater distance from the black hole (e.g. $1000R_s$ instead of $10R_s$). Nonetheless the detection of the 6.7 keV absorption line in NGC 3783 adds to the growing number of cases where high ionization iron K-shell absorption features have been detected. For those AGN where high velocity X-ray iron absorption features have been measured, a large mass outflow rate is often required (typically > 1 $M_\odot$ year^{-1}), of the order of (or even greater than) the actual accretion rate required to power the bolometric luminosity of the sources, e.g. see the discussion in King & Pounds (2003). Similarly, we can also calculate the mass outflow rate required to power the high ionization absorber in NGC 3783, assuming an outflow velocity of 10^3 km s^{-1} (i.e. consistent with the soft X-ray absorber). For a constant velocity outflow, the mass outflow rate will be:-

$$\dot{M}_{\rm out} = \Omega n R^2 v m_{\rm p}$$

where Ω is the solid angle subtended by the absorber and $m_{\rm p}$ is the proton mass. For the iron absorber parameters derived in NGC 3783 (and assuming $\Omega \sim \pi$ steradian), the mass outflow rate is $\dot{M}_{\rm out} = 0.1 M_\odot$ year^{-1}. This is of the same order as the expected accretion rate required to power the observed bolometric luminosity of NGC 3783 (assuming $L_{bol} = 5 \times 10^{44}$ erg s^{-1} at 5% accretion efficiency). Note that if the soft X-ray component of the warm absorber does reside at parsec scale distances, then the mass outflow rate required to sustain this material is even higher, e.g. see the calculation in Behar et al. (2003), of the order 10 $M_\odot$ year^{-1}.

Indeed the large AGN mass outflow rates that are now emerging from the X-ray spectroscopic observations suggest that the role of outflows in AGN are becoming increasingly important. If the outflows are a relatively persistent phenomenon, which is likely as the warm absorbers appear to reside in >50% of Seyfert galaxies (Reynolds 1997), then a large proportion of the matter feeding the AGN may in fact be required to sustain the outflowing material. The implication of this is that lifetime of the AGN within a particular galaxy is likely to be shorter than expected, unless the

source of fuel can be replenished. Not only may the outflows be important in shaping the evolution of the AGN, but they may also play an important role in regulating the bulge mass of the host galaxy, potentially providing an important feedback between the mass of the black hole and the galaxy bulge (Magorrian et al. 1998; Gebhardt et al. 2000; Ferrarese & Merritt 2000). Furthermore if the kinetic energy of the outflows are substantial, particularly in the high velocity cases, then this may even provide a potential heating mechanism for the IGM, perhaps accounting for the relative lack of cool gas at the center of some massive galaxy clusters (Bohringer et al. 2002).

7. Acknowledgments

This paper is based on observations obtained with XMM-Newton, an ESA science mission with instruments and contributions directly funded by ESA Member States and the USA (NASA). We would like to thank Richard Mushotzky and Simon Vaughan for discussions and feedback. T.J. Turner and T. Yaqoob acknowledge support in the form of NASA grants, NAG5-7538 and NAG5-10769 respectively.

REFERENCES

Antonucci, A., 1993, ARA&A, 31, 473

Behar, E., et al. 2003, ApJ, in press

Blustin, A.J., Branduardi-Raymont, G., Behar, E., Kaastra, J.S., Kahn, S.M., Page, M.J., Sako, M., & Steenbrugge, K.C. 2002, A&A, 393, 453

Bohringer, H., Matsushita, K., Churazov, E., Ikebe, Y., & Chen, Y. 2002, A&A, 382, 804

Chartas, G., Brandt, W.N., Gallagher, S.C., & Garmire, G.P. 2002, ApJ, 579, 163

Chartas, G., Brandt, W.N., & Gallagher, S.C. 2003, ApJ, in press (astro-ph/0306125)

De Rosa, A., Piro, L., Fiore, F., Grandi, P., Maraschi, L., Matt, G., Nicastro, F., & Petrucci, P.O. 2002, A&A, 387, 838

Dickey, J.M., & Lockman, F.J. 1990, ARA&A, 28, 215

Elvis, M. ApJ, 2000, 545, 63

Fabian, A.C., Rees, M.J., Stella, L., & White, N.E. 1989, MNRAS, 238, 729

Fabian, A.C., Vaughan, S., Nandra, K., Iwasawa, K., Ballantyne, D.R., Lee, J.C., De Rosa, A., Turner, A., & Young, A.J. 2002, MNRAS, 335, L1

Ferrarese, L., & Merritt, D. 200, ApJ, 539, L9

Gebhardt, K., et al. 2000, ApJ, 539, L13

George, I.M., & Fabian, A.C. 1991, MNRAS, 249, 352

George, I.M., Turner, T.J., & Netzer, H. 1995, ApJ, 438, L67

George, I.M., Turner, T.J., Mushotzky, R., Nandra, K., & Netzer, H. 1998, ApJ, 503, 174

Ghisellini, G., Haardt, F., & Matt, G. 1994, MNRAS, 267, 743

Kallman, T., Liedahl, D., Osterheld, A., Goldstein, W., & Kahn, S. 1996 ApJ, 465, 994

Kaspi, S., Brandt, W.N., Netzer, H., Sambruna, R., Chartas, G., Garmire, G.P., & Nousek, J.A. 2000, ApJ, 535, L17

Kaspi, S., Brandt, W.N., Netzer, H., George, I.M., Chartas, G., Behar, E., Sambruna, R., Garmire, G., & Nousek, J.A. 2001, ApJ, 554, 216

Kaspi, S., et al. 2002, ApJ, 574, 643

King, A., & Pounds, K.A. 2003, MNRAS, in press (astro-ph/0305541)

Krongold, Y. et al., 2003, ApJ, in press

Magdziarz, P., & Zdziarski, A. 1995, MNRAS, 273, 837

Magorrian, J., et al. 1998, AJ, 115, 2285

Matt, G., Guainazzi, M., Perola, G.C., Fiore, F., Nicastro, F., Cappi, M., & Piro, L. 2001, A&A, 377, L31

McHardy, I.M., Lawrence, A., Pye, J.P., & Pounds, K.A. 1981, MNRAS, 197, 893

Nandra, K., & Pounds, K.A., 1994, MNRAS, 268, 405

Nandra, K., George, I.M., Turner, T.J., Fukazawa, Y. 1996, ApJ, 464, 165

Nandra, K., George, I.M., Mushotzky, R.F., Turner, T.J., & Yaqoob, T. 1997, ApJ, 477, 602

Nandra, K., George, I.M., Mushotzky, R.F., Turner, T.J., Yaqoob, T. 1999, ApJ, 523, L17

Nayakshin, S., & Kallman, T.R. 2001, ApJ, 546, 406

Netzer, H., et al. 2003, ApJ, in press

Onken, C.A., & Peterson, B.M. 2002, ApJ, 572, 746

Piccinotti, G., Mushotzky, R.F., Boldt, E.A., Holt, S.S., Marshall, F.E., Serlemitsos, P.J., & Shafer, R.A. 1982, ApJ, 253, 485

Pike, C.D., et al. 1996, ApJ, 464, 487

Pounds, K.A., Nandra, K., Stewart, G.C., George, I.M., & Fabian, A.C. 1990, Nature, 344, 132

Pounds, K., Reeves, J., O'Brien, P., Page, K., Turner, M., & Nayakshin, S. 2002, ApJ, 559, 181

Pounds, K.A., & Reeves, J.N, 2002, to appear in the Proceedings of the Symposium on 'New Visions of the X-ray Universe in the XMM-Newton and Chandra Era' (astro-ph/0201436), 26-30 November 2001, ESTEC, The Netherlands

Pounds, K.A., Reeves, J.N., Page, K.L., Edelson, R., Matt, G., & Perola, G. C. 2003, MNRAS, 341, 953

Pounds, K.A., Reeves, J.N., Page, K.L., Wynn, G.A., O'Brien, P.T., 2003, MNRAS, 342, 1147

Pounds, K.A., Reeves, J.N., King, A., Page, K., & O'Brien, P.T. 2003, MNRAS, in press (astro-ph/0303603)

Proga, D., Stone, J.M., & Kallman, T. 2000, ApJ, 543, 686

Reeves, J.N., Turner, M. J. L., Pounds, K.A., O'Brien, P.T., Boller, Th., Ferrando, P., Kendziorra, E., & Vercellone, S. 2001, A&A, 365, L134

Reeves, J.N., O'Brien, P.T., & Ward, M. 2003, ApJL, in press

Reeves, J., 2003, in Active Galactic Nuclei: from Central Engine to Host Galaxy, meeting held in Meudon, France, July 23-27, 2002, Eds.: S. Collin, F. Combes and I. Shlosman. ASP (Astronomical Society of the Pacific), Conference Series, Vol.290, p. 35.

Reynolds, C.S., 1997, MNRAS, 286, 513

Reynolds, C.S., Wilms, J., Begelman, M.C., Staubert, R., & Kendziorra, E. 2003, ApJ, submitted

Reichert, G.A., et al. 1994, ApJ, 425, 582

Schurch, N., Warwick, R.S., Griffiths, R.S., & Sembay, S. 2003, MNRAS, in press

Struder, L., et al. 2001, A&A, 365, L18

Tanaka, Y., et al. 1995, Nature, 375, 659

Turner, M.J.L., et al. 2001, A&A, 365, L27

Turner, T.J., Nandra, K., George, I.M., Fabian, A.C., & Pounds, K.A. 1993, ApJ, 419, 127

Turner, T.J., Mushotzky, R.F., Yaqoob, T., George, I.M., Snowden, S.L., Netzer, H., Kraemer, S.B., Nandra, K., & Chelouche, D. 2002, ApJ, 574, L123

Turner, T.J., Kraemer, S.B., George, I.M., & Reeves, J.N. 2003, ApJ, submitted

Vaughan, S., Fabian, A.C., & Iwasawa, K. 2003, MNRAS, submitted

Wandel, A., Peterson, B.M., & Malkan, M.A., 1999, ApJ, 526, 579

Wilms, J., Allen, A., McCray, R. 2000, ApJ, 542, 914

Wilms, J., Reynolds, C.S., Begelman, M.C., Reeves, J., Molendi, S., Staubert, R., & Kendziorra, E. 2001, MNRAS, 328, L27

Yaqoob, T., George, I.M., Nandra, K., Turner, T.J., Serlemitsos, P.J., & Mushotzky, R. F. 2001, ApJ, 546, 759

Yaqoob, T., George, I.M., Kallman, T.R., Padmanabhan, U., Weaver, K.A., & Turner, T.J., 2003, ApJ, in press

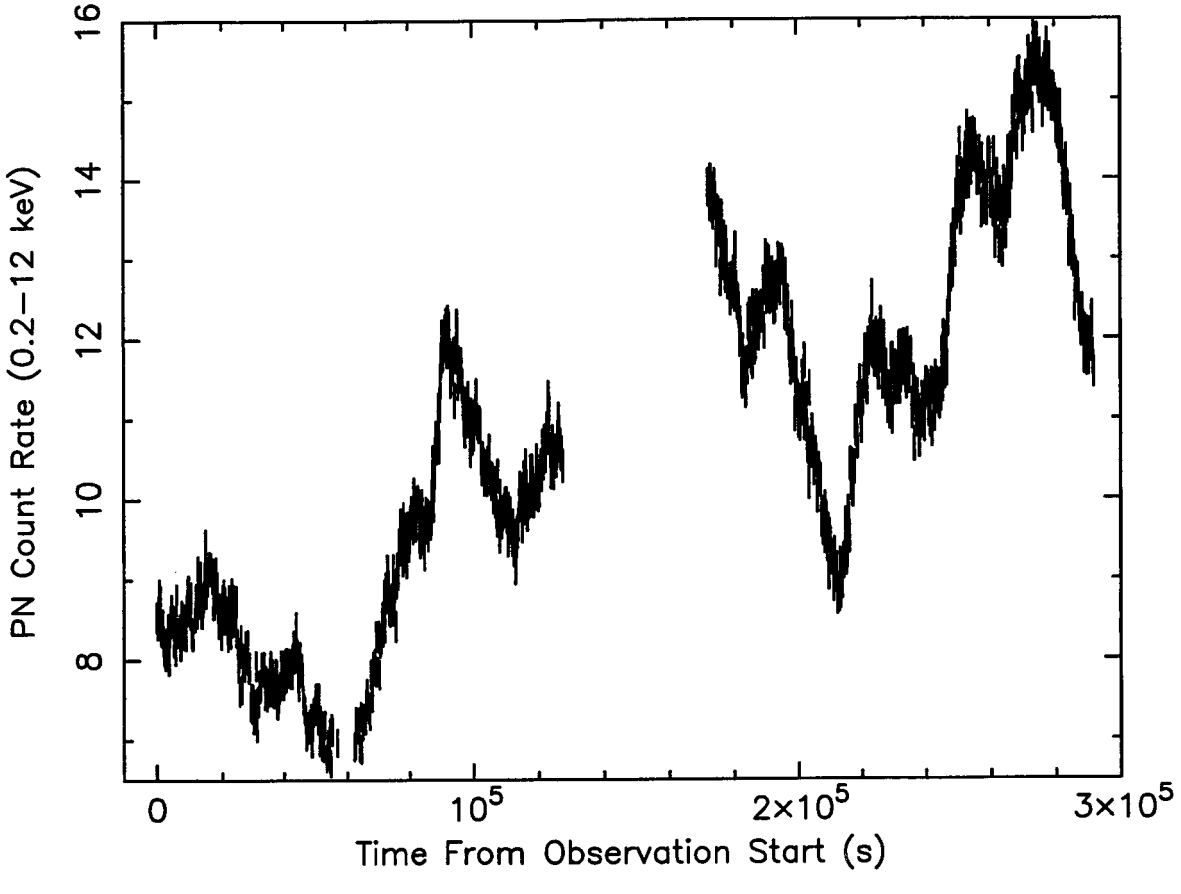

Fig. 1.— The 0.2-12 keV EPIC-pn lightcurve of NGC 3783, observed over two whole *XMM-Newton* orbits. The observation started on 17 November 2001, with a total exposure time (after screening) of $\sim$ 240 ks.

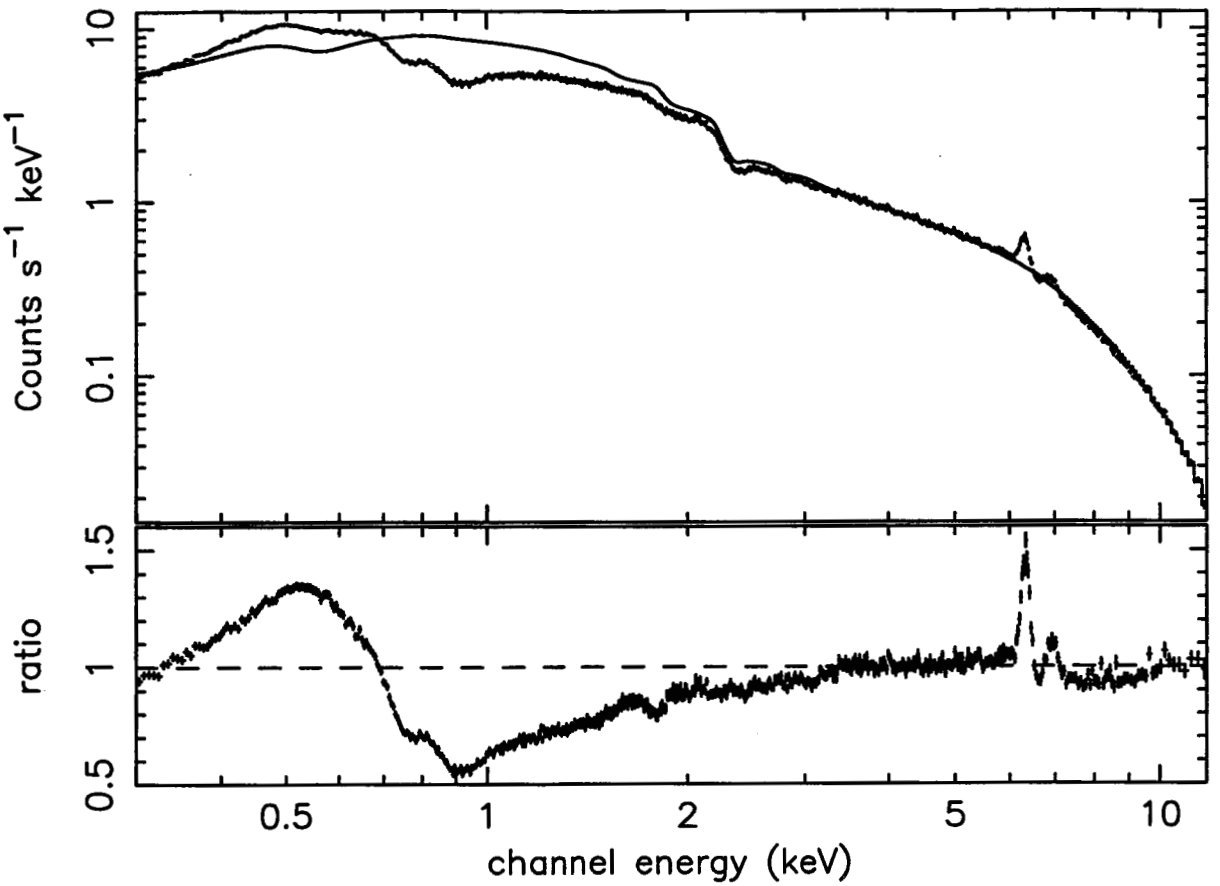

Fig. 2.— The broad-band (0.2-12 keV) EPIC-pn spectrum of NGC 3783. The upper panel shows the data, plotted against a power-law model of photon index $\Gamma = 1.6$ (solid line), which has been convolved through the detector response matrix. The lower panel shows the data/model ratio residuals to this power-law fit. Clear deviations in the iron K-shell band are apparent between 6-7 keV, whilst a deficit of counts (due to the the warm absorber) is present between 0.7-3.0 keV, whilst a weak soft excess over the power-law continuum is observed below 0.5 keV.

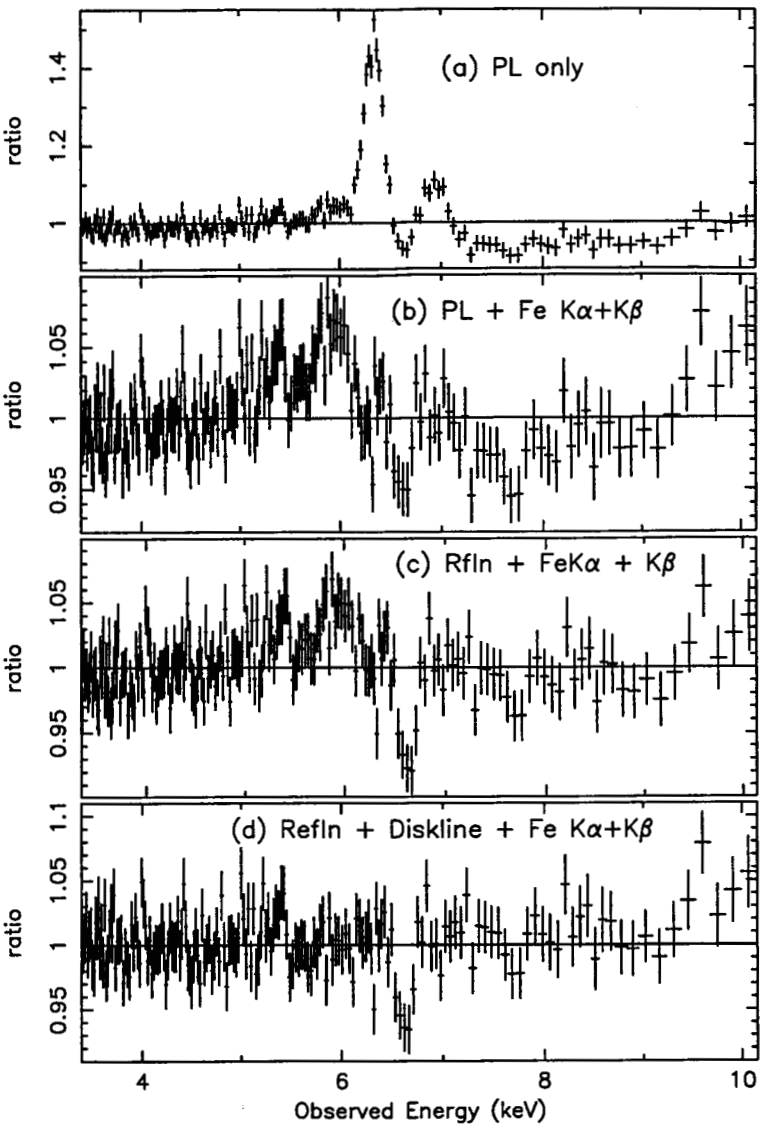

Fig. 3.— Data/model ratio residuals of the 3.5-12.0 keV band spectrum of NGC 3783, in the iron K-shell band. Panel (a) shows the residuals to a simple power-law fit, with Galactic absorption. The two strong peaks due to emission lines at 6.4 and 7.0 keV are readily apparent. Panel (b) shows the residuals after the two Fe emission lines at 6.4 keV and 7.0 keV have been fitted. Panel (c) shows the residuals after the addition of a neutral reflection component with R=1, a weak red-wing to the Fe line is apparent below 6.4 keV. Panel (d) shows the residuals after the addition of a disk emission line component to model the red-wing. A strong absorption line, probably due to Fe XXV, is present at 6.7 keV.

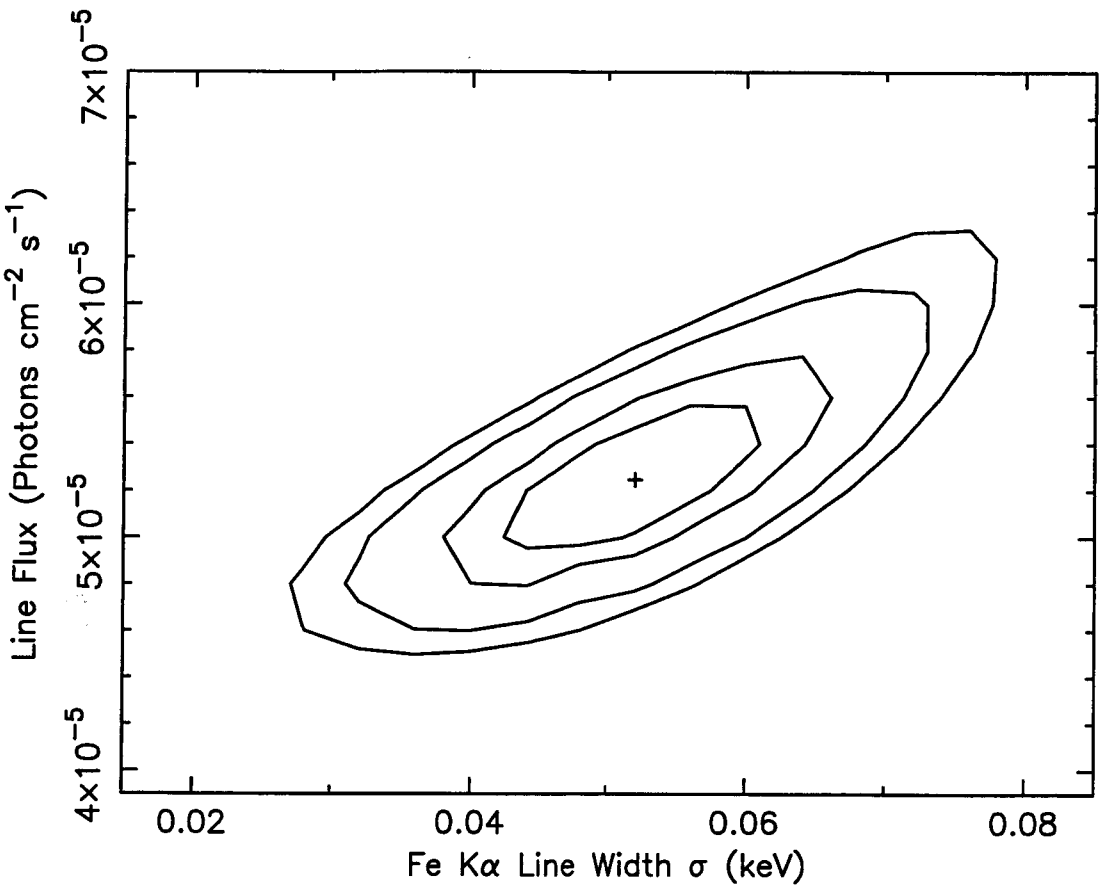

Fig. 4.— Contour plot showing the 68%, 90%, 99% and 99.9% confidence levels of Fe Kα line flux versus line width for the 6.4 keV emission line. The line appears to be resolved by EPIC-pn with a width of 52 ± 10 eV, corresponding to a FWHM velocity width of ~ 5600 km s^{-1}. This places the bulk of the Fe line emission at the broad line region or even further away from the nucleus.

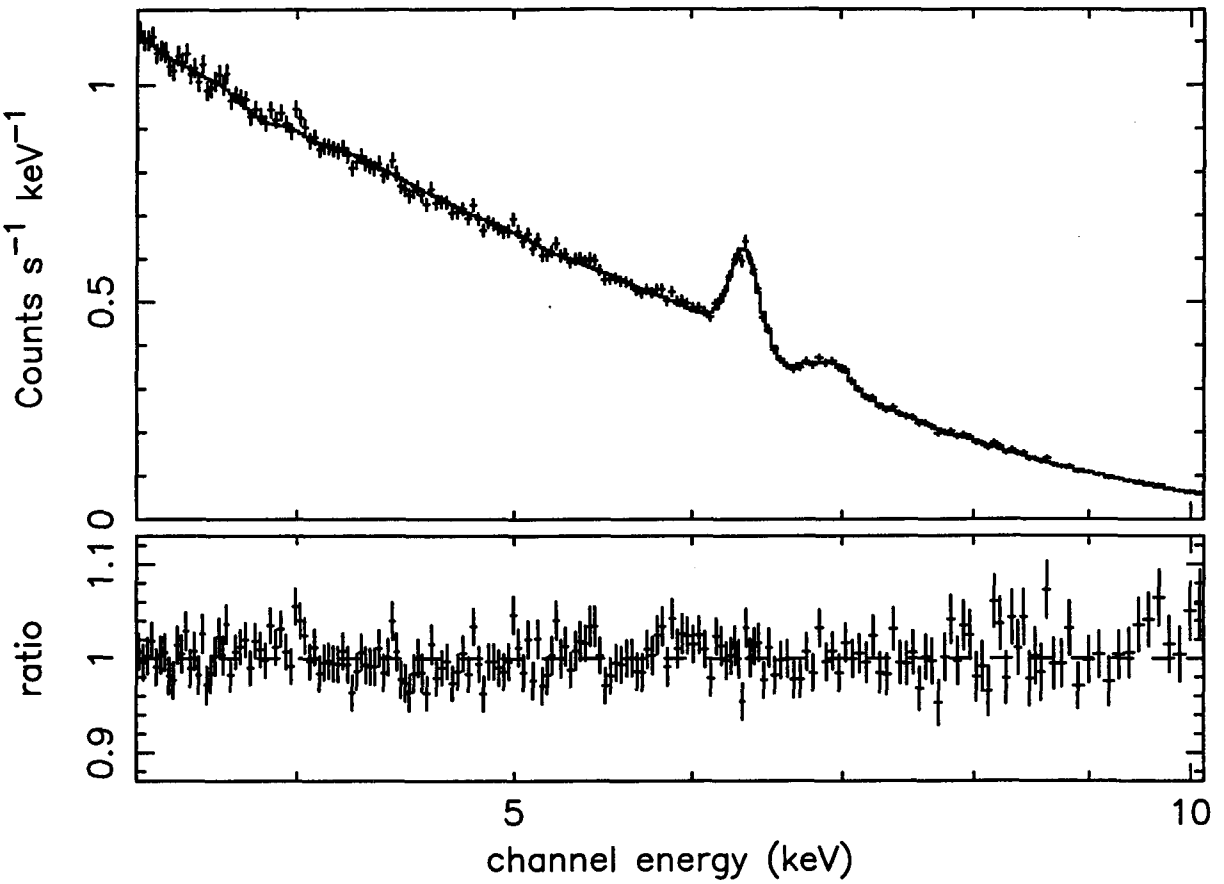

Fig. 5.— The 3.5-12 keV EPIC-pn spectrum (upper panel) and data/model residuals (lower panel) to a fit with a two zone warm absorber, modeled by the XSTAR photoionization code. The two narrow emission lines at 6.4 keV and 7.0 keV have been included in the fit, but the broad red-wing to the iron Kα emission line is no longer required once the absorber has been correctly modeled. A high ionization absorber, with ionization parameter $\log \xi = 2.9 \pm 0.3$ erg cm s^{-1} and a column density of $N_{\rm H} = (4.6 \pm 0.8) \times 10^{22}$ cm^{-2} reproduces the energy and depth of the 6.7 keV absorption line rather well.

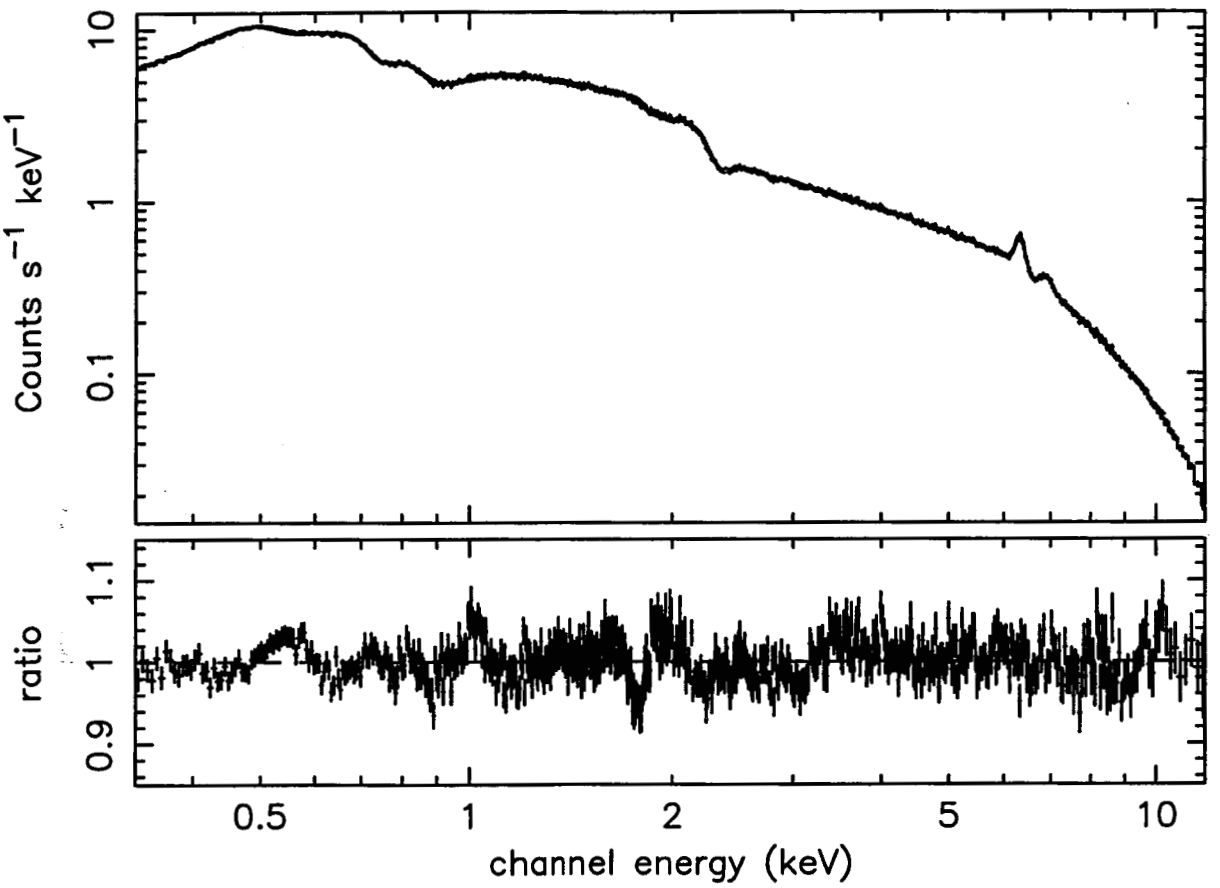

Fig. 6.— The broad-band 0.3-12 keV EPIC-pn spectrum and data/model residuals (lower panel). The spectrum has been modeled with a multiple component warm absorber, including the 2 lower ionization components (with log $\xi \sim 0.3$ and log $\xi \sim 2.4$) modeled by (Blustin et al. 2002) to the RGS data, as well as the high ionization component (with log $\xi \sim 2.9$) responsible for the Fe K-shell absorption. This model fits the overall X-ray spectrum of NGC 3783 well, the remaining data/model residuals are at the 5% level or smaller.

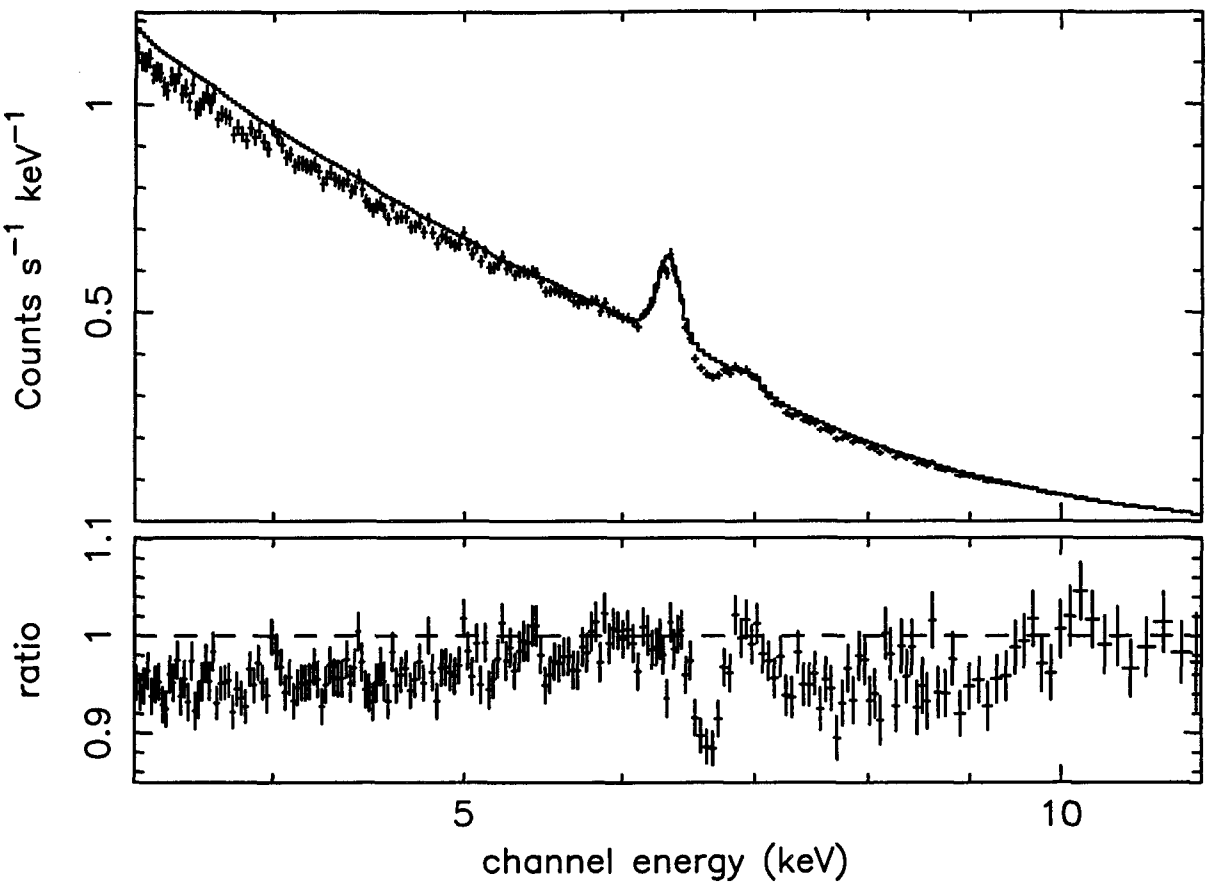

Fig. 7.— The 3.5-12 keV EPIC-pn spectrum and residuals after removing the two zone warm absorber in Figure 5, plotted in order to illustrate the effect of the ionized absorber on the hard X-ray spectrum. The deep absorption line at 6.7 keV is clearly apparent in the residuals, whilst an broad dip is present in the between 7 and 9 keV, due to iron K-shell edge absorption. There is also significant opacity in the absorber below 6 keV, which effects any modeling of the broad iron line.

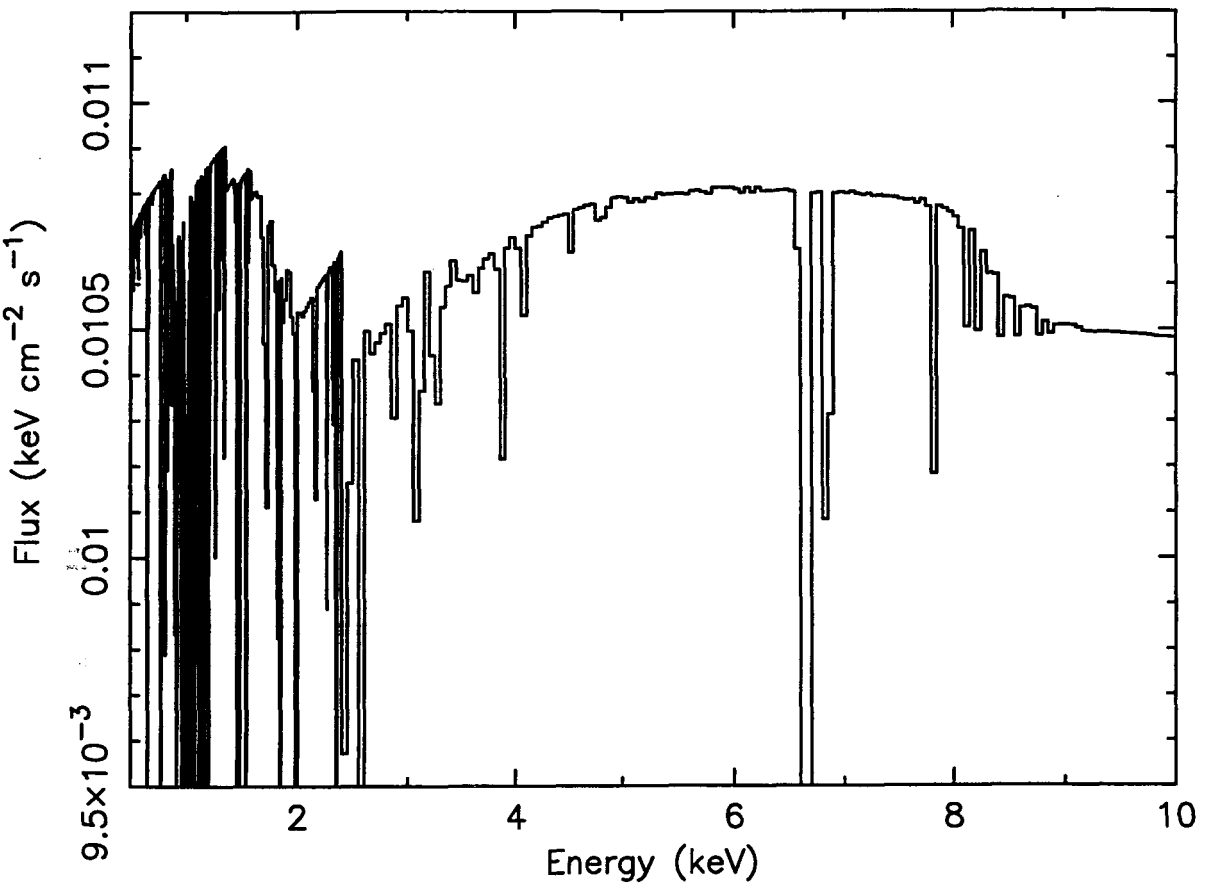

Fig. 8.— The high ionization warm absorber model, fitted to the 3.5-12 keV EPIC-pn spectrum, but normalized to a $\Gamma = 2$ power-law continuum for ease of illustration only. As well as the strong Fe Kα absorption lines that are present near 6.7 keV, the model introduces significant continuum curvature between 3-6 keV, due to recovery from high ionisation K-shell edges and lines from Mg, Si, S, as well as L-shell Fe below 3 keV. Additional opacity is also between 7-9 keV, due to a blend of high ionization Fe K-shell edges and higher series absorption lines, such as Fe Kβ.

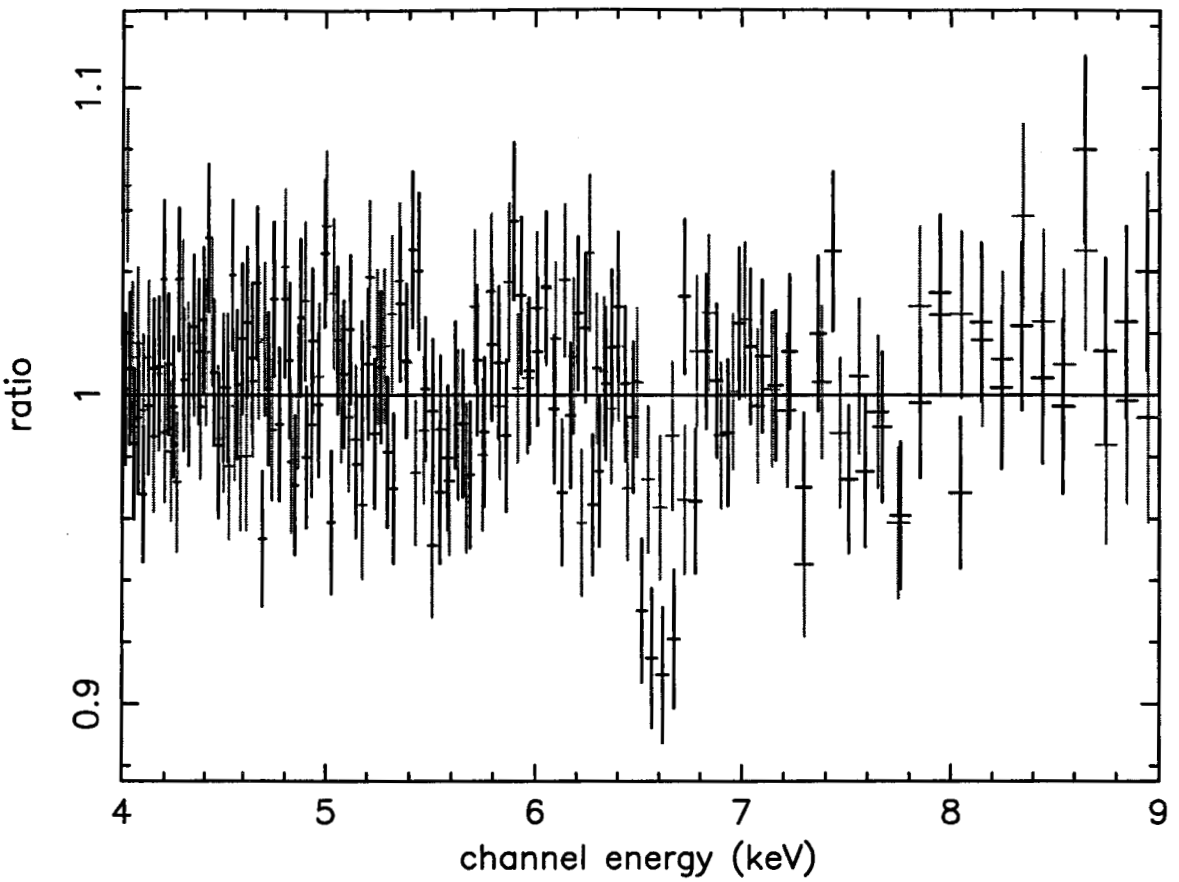

Fig. 9.— The data/model ratio residuals over the iron K-shell band from the two orbits of *XMM-Newton* EPIC-pn data. The first orbit is plotted in greyscale, the second orbit in black. The narrow 6.4 and 7.0 keV emission lines have been modeled in the spectrum. The 6.7 keV absorption line is clearly present in the second orbit of data, but is very weak in the first orbit, indicating that this high ionization absorption component is variable on short timescales, of the order 10^5 s.

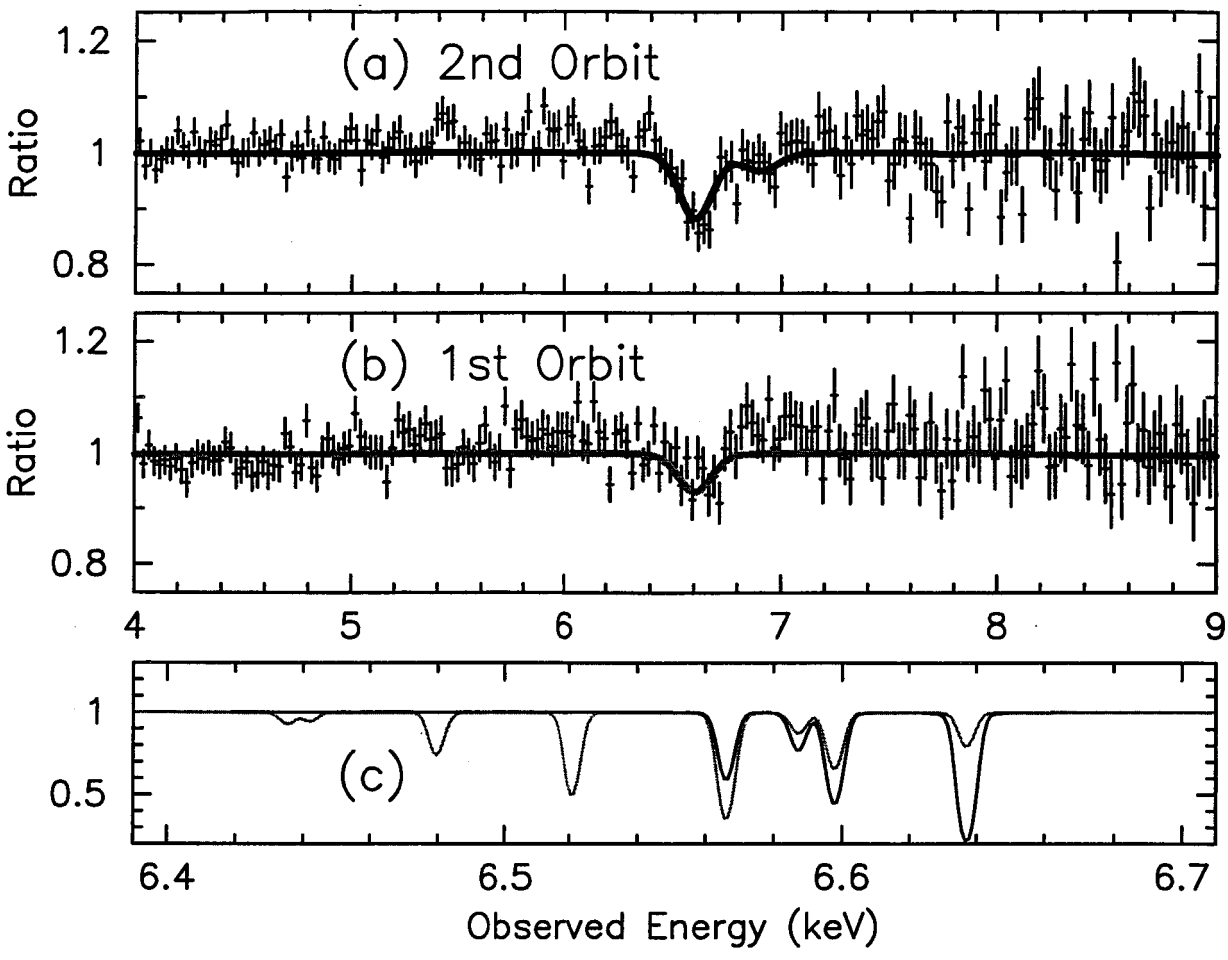

Fig. 10.— Fits to the iron K-shell absorption line in the two seperate *XMM-Newton* orbits. (a) The data (crosses) and absorption line model (solid line), convolved through the EPIC-pn response, to the *XMM-Newton* spectrum during the 2nd orbit. Here, the absorption line is strongest when the continuum flux is higher. It can be modeled with a high ionization absorber, where the Fe XXV resonance ($1s \rightarrow 2p$) line is the strongest line present. (b) The first orbit of data, when the continuum flux is lower and best fit model overlaid (solid grey line). The absorption line is weaker during the 1st orbit, which is consistent with a lower overall ionization for the iron K band absorber. (c) The relative strengths of the absorption lines from Fe XXV to Fe XX (right to left) from the two models shown above; the lines correspond to observed energies of 6.64 keV, 6.59 keV (doublet), 6.565 keV, 6.52 keV, 6.48 keV and 6.44 keV, or rest (lab) frame energies of 6.70 keV, 6.66 keV, 6.63 keV, 6.58 keV, 6.54 keV and 6.50 keV respectively. The high ionization model (for the 2nd orbit) is plotted in black, the lower ionization model (for the 1st orbit) in greyscale. Thus the higher flux 2nd orbit may be dominated by the higher ionization ions (Fe XXIII–XXV), whilst the lower ionization species (Fe XX–XXIII) are more dominant in the lower flux 1st orbit spectrum.

Table 1. Table of iron line spectral fits.

Fit	Γ	Line	E^{a}	σ^{b}	EW^{c}	χ^2/dof	P^{d}
1.	1.62 ± 0.01	Fe Kα	6.39 ± 0.01	57 ± 8	123 ± 6	1589/1287	1.4×10^{-8}
		Fe Kβ/Fe XXVI	7.00 ± 0.02	53 ± 23	34 ± 5		
2.	1.62 ± 0.01	Fe Kα	6.39 ± 0.01	57 ± 8	123 ± 6	1591/1287	1.15×10^{-8}
		Fe XXVI	6.96 ± 0.02	57[e]	20 ± 5		
		Fe Kβ	7.06[e]	57[e]	16[e]		
3.	1.73 ± 0.01	Fe Kα	6.39 ± 0.01	47 ± 8	109 ± 5	1492/1287	5.6×10^{-5}
		Fe XXVI	7.00 ± 0.04	47[e]	12 ± 4		
		Fe Kβ	7.06[e]	47[e]	14[e]		
4.	1.73 ± 0.01	Fe Kα	6.40 ± 0.01	53 ± 8	107 ± 8	1324/1282	2.0×10^{-1}
		Fe XXVI	6.98 ± 0.04	53[e]	17 ± 5		
		Fe Kβ	7.06[e]	53[e]	14[e]		
		Fe XXV absn	6.67 ± 0.04	10[e]	17 ± 5		
		Diskline	6.4[e]		58 ± 12		

[a]Energy of the Fe line in units of keV.

[b]1σ width of the line in eV.

[c]Equivalent width of the line in eV.

[d]Null hypothesis probability that the fit statistic is acceptable.

[e]Parameter value is fixed, or tied to that of another fit parameter

Note. — Fit 1 consists of a power-law plus 2 Gaussian emission lines. Fit 2 is a power-law plus 3 Gaussian emission lines. Fit 3 is a power-law plus 3 Gaussian emission lines and neutral reflection component (the XSPEC model PEXRAV with $R = 1$). Fit 4 consists of a power-law, plus three Gaussian emission lines, a neutral reflection component, a disk emission line (the DISKLINE model in xspec), as well as a Gaussian shaped absorption line.